EXOPLANET ATMOSPHERES

Ground-based detection of an extended helium atmosphere in the Saturn-mass exoplanet WASP-69b

Lisa Nortmann[1,2]*, Enric Pallé[1,2], Michael Salz[3], Jorge Sanz-Forcada[4], Evangelos Nagel[3], F. Javier Alonso-Floriano[5], Stefan Czesla[3], Fei Yan[6], Guo Chen[1,2,7], Ignas A. G. Snellen[5], Mathias Zechmeister[8], Jürgen H. M. M. Schmitt[3], Manuel López-Puertas[9], Núria Casasayas-Barris[1,2], Florian F. Bauer[8,9], Pedro J. Amado[9], José A. Caballero[4], Stefan Dreizler[8], Thomas Henning[6], Manuel Lampón[9], David Montes[10], Karan Molaverdikhani[6], Andreas Quirrenbach[11], Ansgar Reiners[8], Ignasi Ribas[12,13], Alejandro Sánchez-López[9], P. Christian Schneider[3], María R. Zapatero Osorio[14]

Hot gas giant exoplanets can lose part of their atmosphere due to strong stellar irradiation, and these losses can affect their physical and chemical evolution. Studies of atmospheric escape from exoplanets have mostly relied on space-based observations of the hydrogen Lyman-α line in the far ultraviolet region, which is strongly affected by interstellar absorption. Using ground-based high-resolution spectroscopy, we detected excess absorption in the helium triplet at 1083 nanometers during the transit of the Saturn-mass exoplanet WASP-69b, at a signal-to-noise ratio of 18. We measured line blueshifts of several kilometers per second and posttransit absorption, which we interpret as the escape of part of the atmosphere trailing behind the planet in comet-like form.

In recent years, high-resolution spectroscopy has become a frequently used tool for investigating exoplanet atmospheres (*1*–*4*). Numerous stable high-resolution spectrographs have been deployed on telescopes specifically for exoplanetary science (*5*–*8*). One of these spectrographs is CARMENES (Calar Alto high-Resolution search for M dwarfs with Exoearths with Near-infrared and optical Échelle Spectrographs) (*8*) at the 3.5-m telescope of the Calar Alto Observatory. The spectrograph simultaneously covers the visible wavelength range from 0.52 to 0.96 μm and the near-infrared range from 0.96 to 1.71 μm. The near-infrared coverage provides access to exoplanet atmospheric features that cannot be observed in the visible range, including the triplet of metastable He I lines around 1083 nm. This feature has been proposed as a tracer for atmospheric evaporation (*9*), a process whereby intense x-ray (~0.5 to 10.0 nm) and extreme ultraviolet (EUV) (10.0 to 92.0 nm) irradiation from a host star causes atmospheres of hot gas exoplanets to expand, resulting in a bulk mass flow away from the planet. The continuous mass loss most strongly affects small sub-Neptune–sized planets and may be capable of removing their entire volatile atmosphere (*10*). Helium absorption at 1083 nm is sensitive to the low-density gas in an evaporating atmosphere (*9*, *11*, *12*), and its observation is not affected by absorption in the foreground interstellar medium, which hampers studies of the neutral hydrogen Lyman-α (Lyα) line (*9*). He I absorption has been detected in a transmission spectrum of the exoplanet WASP-107b using data from the Hubble Space Telescope (*13*). However, the low resolution prevented a detailed study of the line triplet, including its shape, depth, and temporal behavior.

The Saturn-mass exoplanet WASP-69b orbits an active star with a period of 3.868 days (*14*). It is a suitable target for atmospheric studies, due to its large atmospheric scale height and high planet-to-star radius ratio, facilitating the detection of 5.8 ± 0.3% excess absorption in the Na D line (*15*). We used the CARMENES spectrograph to observe two transits of WASP-69b on 22 August 2017 and 22 September 2017 (night 1 and night 2, respectively) (see table S1 for the observing log). The observations spanned approximately 4 hours for each epoch, which covered the full transit and provided a before- and after-transit baseline. In total, 66 spectra were recorded, 31 of them out-of-transit spectra.

The wavelength region surrounding the He I feature is affected by emission and water vapor absorption lines originating from within Earth's atmosphere (fig. S1). Although these lines are spectrally separated from the He I triplet, we corrected for the effect of water absorption using the European Southern Observatory (ESO) tool Molecfit (*16*) and for the sky emission lines using an empirical model derived from the data (*17*). After this correction, we performed continuum normalization and brought the spectra to the stellar velocity rest frame. We then computed a master out-of-transit spectrum (F_{out}), which was used to normalize all spectra, following

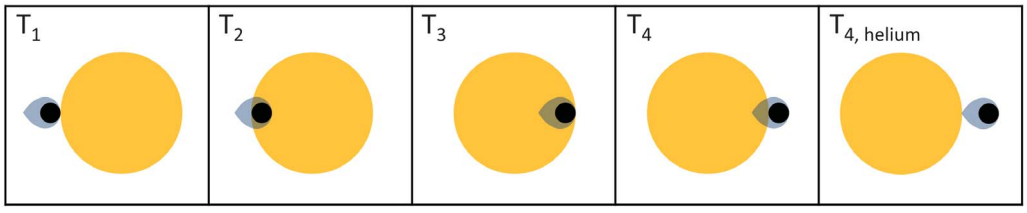

Fig. 1. Illustration of the exoplanet WASP-69b (black) and its extended helium atmosphere (gray-blue) at the different contact points. Shown are the first (T_1), second (T_2), third (T_3), and fourth (T_4) contacts of the broadband planet transit and also the moment when the tail has passed the stellar disk, $T_{4,\ helium}$, 22 ± 3 min after T_4.

[1]Instituto de Astrofísica de Canarias, Vía Láctea s/n, 38205 La Laguna, Tenerife, Spain. [2]Departamento de Astrofísica, Universidad de La Laguna, 38206 La Laguna, Tenerife, Spain. [3]Hamburger Sternwarte, Universität Hamburg, Gojenbergsweg 112, 21029 Hamburg, Germany. [4]Centro de Astrobiología, Consejo Superior de Investigaciones Científicas—Instituto Nacional de Técnica Aeroespacial (CSIC-INTA), European Space Astronomy Centre campus, Camino bajo del castillo s/n, 28692 Villanueva de la Cañada, Madrid, Spain. [5]Leiden Observatory, Leiden University, Postbus 9513, 2300 RA, Leiden, Netherlands. [6]Max-Planck-Institut für Astronomie, Königstuhl 17, 69117 Heidelberg, Germany. [7]Key Laboratory of Planetary Sciences, Purple Mountain Observatory, Chinese Academy of Sciences, Nanjing 210008, China. [8]Institut für Astrophysik, Georg-August-Universität, 37077 Göttingen, Germany. [9]Instituto de Astrofísica de Andalucía, Consejo Superior de Investigaciones Científicas (CSIC), Glorieta de la Astronomía s/n, 18008 Granada, Spain. [10]Departamento de Astrofísica y Ciencias de la Atmósfera, Facultad de Ciencias Físicas, Universidad Complutense de Madrid, 28040 Madrid, Spain. [11]Landessternwarte, Zentrum für Astronomie der Universität Heidelberg, Königstuhl 12, 69117 Heidelberg, Germany. [12]Institut de Ciències de l'Espai, Consejo Superior de Investigaciones Científicas (CSIC), Campus Universitat Autònoma de Barcelona, c/ de Can Magrans s/n, 08193 Bellaterra, Barcelona, Spain. [13]Institut d'Estudis Espacials de Catalunya, 08034 Barcelona, Spain. [14]Centro de Astrobiología, Consejo Superior de Investigaciones Científicas—Instituto Nacional de Técnica Aeroespacial (CSIC-INTA), Crta. de Ajalvir km 4, E-28850 Torrejón de Ardoz, Madrid, Spain.
***Corresponding author. Email: nortmann.astro@gmail.com**

standard analysis methods (*1*, *15*). The resulting residual spectra contain the exoplanet absorption signal (fig. S2). We shifted them into the planetary rest frame and computed the transmission spectrum by co-adding all residual in-transit spectra (F_{in}/F_{out}) obtained between second and third contact (Fig. 1), i.e., when the planet disk was fully in front of the stellar disk.

The combined transmission spectrum for the two nights is shown in Fig. 2. An excess absorption in the He I line at the level of 3.59 ± 0.19% was detected. The given uncertainty corresponds to 1 standard deviation (1σ) of the continuum flux. The signal was detected separately in each visit at 3.96 ± 0.25% (1σ) and 3.00% ± 0.31% (1σ) for nights 1 and 2, respectively (fig. S3). We modeled the transmission spectrum with three Gaussian functions with fixed amplitude ratios and relative wavelengths according to theoretical values for the He I triplet (*18*, *19*). We fitted a common line width, Doppler shift, and intensity of the lines (*17*) and determined parameter uncertainties by Markov chain Monte Carlo sampling (fig. S4). The best-fitting model indicates a net blueshift of −3.58 ± 0.23 km s^{-1} (where the uncertainty corresponds to the standard deviation of the posterior probability distribution).

To examine the behavior of the helium absorption over time, we constructed a light curve by summing the flux within a 0.04-nm-wide passband centered on the blueshifted core of the He I feature for each residual spectrum in the planet rest frame (*15*). The resulting light curves for each of the two nights are shown in Fig. 3. The helium absorption began shortly after the planet ingress, with no observable pretransit absorption, and lasted for 22 ± 3 min after the transit ended (fig. S5). This light curve behavior does not depend on the width of the chosen passband. By fitting the Rossiter-McLaughlin effect (RME), a deformation of the stellar lines caused by the planet occulting different parts of the rotating stellar surface during transit, for our visible channel radial velocity data (*17*) (fig. S6), we obtained midtransit times consistent with the known planet orbit. The signal of the RME corresponded with the predicted broadband transit duration of 2.23 hours (*14*), so we can be confident that the observed post-transit helium absorption is real. We used the RME curve to estimate the potential contamination of the transmission spectrum by the corresponding deformation of the stellar lines during transit; we found that the impact was negligible (*17*) (fig. S7). The He I D_3 line at 587.6 nm and the Ca II infrared triplet (IRT) at 849.8, 854.2, and 866.2 nm, both indicators of stellar activity, showed no sign of active regions (*17*) (fig. S8). The time delay of the helium ingress and egress indicates that the distribution of helium around the planet is asymmetrical and that a cloud of gas is trailing the planet along its orbit (Fig. 1). We calculated the length of this tail as ~170,000 km, i.e., 2.2 times the planet radius (longer if tilted with respect to the planet's orbit). Acceleration of the tail material away from the planet could be the cause of the blueshifted absorption. This hypothesis is supported by the larger measured net blueshift of −10.69 ± 1.00 km s^{-1} when only the helium tail is occulting the stellar disk (fig. S9). The tail length and velocities suggest that helium is escaping the planet (*17*).

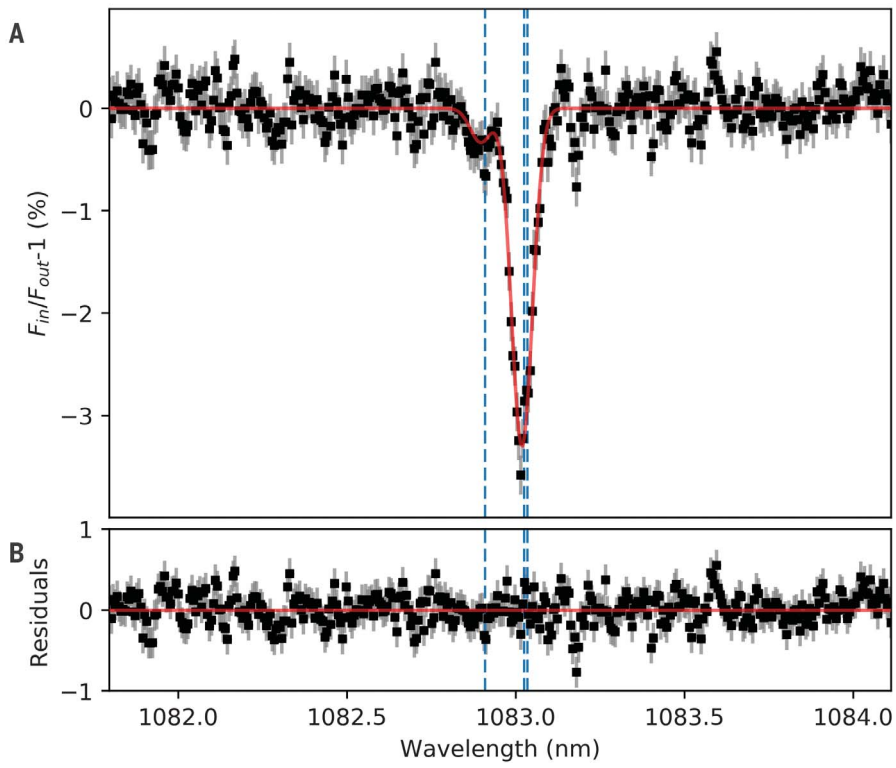

Fig. 2. Transmission spectrum between the second and third contacts of WASP-69b, showing planetary absorption in the He I triplet at 1083 nm. (**A**) The excess absorption of helium in the weighted-mean averaged transmission spectrum (black points) from two transit observations of WASP-69b (22 August 2017 and 22 September 2017) (see Fig. 1). The best-fitting model (red line) shows a net blueshift of −3.58 ± 0.23 km s^{-1}. The predicted positions of the helium triplet lines (1082.909 nm, 1083.025 nm, and 1083.034 nm) are indicated as vertical dashed blue lines. (**B**) The residuals of the data after subtraction of the model are shown in black, and the red line indicates the zero level.

We also analyzed CARMENES transit observations of the hot Jupiter-mass exoplanets HD 189733b and HD 209458b, the extremely hot planet KELT-9b, and the warm Neptune-sized exoplanet GJ 436b (fig. S10). GJ 436b and HD 209458b both show evaporation of hydrogen in the Lyα line (*20*, *21*), and KELT-9b is surrounded by a large cloud of evaporating hydrogen absorbing in the Balmer Hα line at 656.28 nm (*22*). GJ 436b and HD 209458b are predicted to have large absorption depths in the He I line (~8% and ~2%, respectively) (*9*), although a previous study of HD 209458b did not detect any absorption (*23*). We did not detect He I absorption for most of these planets, with 90% confidence upper limits of 0.41% for GJ 436b, 0.84% for HD 209458b [i.e., in disagreement with the predicted levels (*9*)], and 0.33% for KELT-9b (fig. S10). However, we did detect helium absorption in HD 189733b at the level of 1.04 ± 0.09% (*24*). A companion paper reports a similar detection of helium absorption for the warm Neptune-sized planet HAT-P-11b (*25*). For our detections, we calculated the equivalent height of the He I atmosphere δ_{Rp}, i.e., the height of an opaque atmospheric layer that would produce the observed absorption signal (table S2). For both WASP-69b and HD 189733b, we found δ_{Rp} to be ~80 times as large as the atmospheric scale height H_{eq} calculated for the respective planet's deep atmosphere, i.e., in hydrostatic equilibrium (*17*). For the other three planets, our upper limits correspond to no detections of features above ~40 H_{eq}.

Why do similar hot gas exoplanets show such a range of helium absorption values? The expansion of the escaping planetary atmosphere depends on parameters like the EUV irradiation and the planetary density (*26*), but the population of the helium triplet state depends on the irradiation at wavelengths <50.4 nm (*9*). Whereas GJ 436b and HD 209458b orbit very quiet stars (*27*, *28*), the hosts of the planets in which helium is detected, i.e., WASP-69, HD 189733, HAT-P-11, and WASP-107, are all relatively active stars (*14*, *15*, *29*, *30*). For Fig. 4A, we plotted the

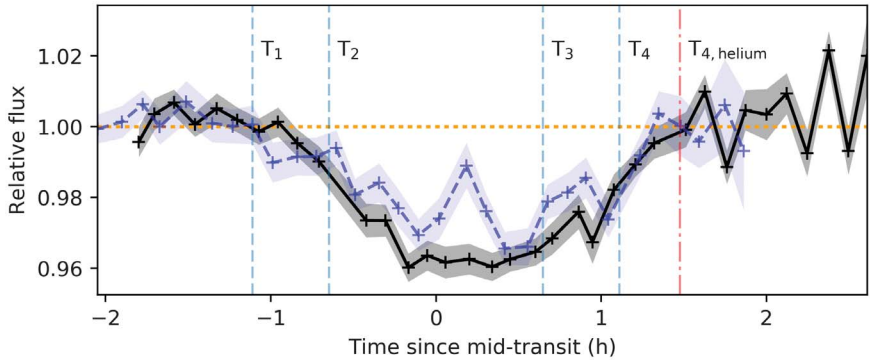

Fig. 3. Spectrophotometric transit light curves of WASP-69b. We integrated the spectral flux in a 0.04-nm-wide bin around the core of the planetary He I line for every observed spectrum over two transits, normalized by the continuum flux outside of the absorption feature. The first (T_1), second (T_2), third (T_3), and fourth (T_4) contacts of the planet transit are marked by dashed vertical lines. Two individual transit light curves are shown in black (night 1) and blue (night 2). The drop in flux from the continuum transit has already been removed, leaving the excess absorption due to helium. The continuum behavior is indicated by the horizontal yellow dotted line. The 1σ uncertainty intervals are shown as light blue and gray shaded regions. The excess absorption lasts until well after the stellar occultation by the planet has ended (T_4), indicating that absorbing material is still in front of the star. We find the excess absorption ends 22 ± 3 min after the planet's egress ($T_{4,\ helium}$, vertical red dash-dotted line).

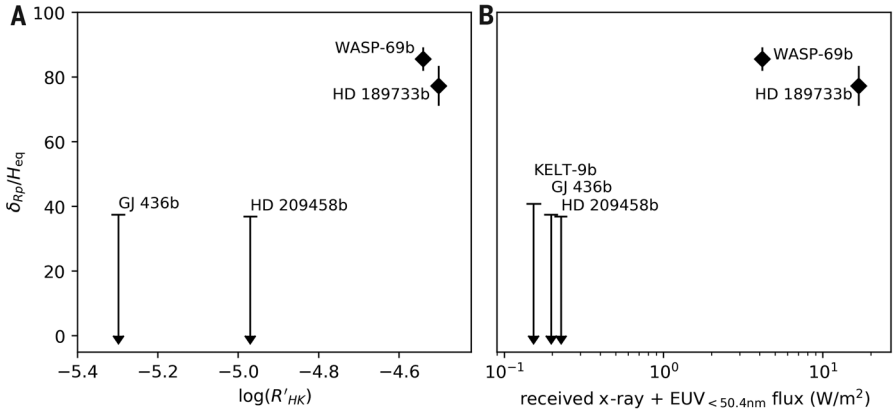

Fig. 4. Detected signals as a function of host star activity and received XUV_{He} irradiation. The equivalent heights of the He I atmosphere δ_{Rp}, normalized by one atmospheric scale height of the respective planet's lower atmosphere H_{eq}, are shown. For the two detections we plotted 1σ error bars, and for the nondetections we plotted upper limits corresponding to a 90% confidence level. (**A**) δ_{Rp}/H_{eq} as a function of the host star activity index $\log(R'_{HK})$, where larger values indicate stronger stellar activity (*31*). The KELT-9 system is not plotted, because its $\log(R'_{HK})$ is not known. (**B**) δ_{Rp}/H_{eq} as a function of stellar flux with a wavelength <50.4 nm at the distance of the planet orbit. The two strong detections of an extended helium atmosphere occur for the two planets having more active host stars and higher planetary XUV_{He} irradiation.

normalized absorption altitude of helium δ_{Rp}/H_{eq} against the stellar activity index $\log(R'_{HK})$ (*31*). Our sample size was limited, but the detections succeeded for the planets with the more active stellar hosts, hinting at a relation between He I detectability and host star activity.

Low-mass stars (F-, G-, K-, and M-types) have a convective layer that, in combination with stellar rotation, produces phenomena associated with magnetic activity. The exterior layers of low-mass stars are (from inside to outside) photosphere, chromosphere, transition region, and corona. In general, activity in the chromosphere is detected in spectral features such as the activity indicator Ca II H and K doublet lines at 393.4 and 396.8 nm, whereas the transition region and the corona produce emission in x-ray and EUV. The metastable 2^3S helium triplet state, which is the lower level of the observed absorption lines, is populated via radiative ionization of He I by photons with wavelengths <50.4 nm followed by recombination (*32*). Thus, a higher x-ray and EUV (<50.4 nm, hereafter XUV_{He}) irradiation level should enhance the formation of the He I triplet in atmospheres of hot gas planets. We calculated the XUV_{He} flux received by all discussed planets (table S3) at the separation of their orbit (*17*) (table S4). For Fig. 4B, we plotted the normalized He I atmospheric altitude δ_{Rp}/H_{eq} for our measurements as a function of the XUV_{He} flux. The line is detected for the planets receiving the largest combined XUV_{He} irradiation. These results indicate a dependence of the detectability of He I in planetary atmospheres on intense x-ray and EUV emission from the parent star.

REFERENCES AND NOTES

1. I. A. G. Snellen, R. J. de Kok, E. J. W. de Mooij, S. Albrecht, *Nature* **465**, 1049–1051 (2010).
2. M. Brogi *et al.*, *Nature* **486**, 502–504 (2012).
3. A. C. Lockwood *et al.*, *Astrophys. J.* **783**, L29 (2014).
4. M. Brogi *et al.*, *Astron. Astrophys.* **615**, A16 (2018).
5. E. Oliva *et al.*, in *Proceedings of the Society of Photo-Optical Instrumentation Engineers Conference Series*, I. S. McLean, M. Iye, Eds. (SPIE, 2006), vol. 6269, p. 626919.
6. S. Mahadevan *et al.*, in *Ground-Based and Airborne Instrumentation for Astronomy IV*, I. S. McLean, S. K. Ramsay, H. Takami, Eds. (SPIE, 2012), vol. 8446, p. 84461S.
7. É. Artigau *et al.*, in *Ground-Based and Airborne Instrumentation for Astronomy V*, S. K. Ramsay, I. S. McLean, H. Takami, Eds. (SPIE, 2014), vol. 9147, p. 914715.
8. A. Quirrenbach *et al.*, in *Ground-Based and Airborne Instrumentation for Astronomy V*, J. Evans, L. Simard, H. Takami, Eds. (SPIE, 2014), vol. 9147, p. 91471F.
9. A. Oklopčić, C. M. Hirata, *Astrophys. J.* **855**, L11 (2018).
10. M. S. Lundkvist *et al.*, *Nat. Commun.* **7**, 11201 (2016).
11. S. Seager, D. D. Sasselov, *Astrophys. J.* **537**, 916–921 (2000).
12. J. D. Turner, D. Christie, P. Arras, R. E. Johnson, C. Schmidt, *Mon. Not. R. Astron. Soc.* **458**, 3880–3891 (2016).
13. J. J. Spake *et al.*, *Nature* **557**, 68–70 (2018).
14. D. R. Anderson *et al.*, *Mon. Not. R. Astron. Soc.* **445**, 1114–1129 (2014).
15. N. Casasayas-Barris *et al.*, *Astron. Astrophys.* **608**, A135 (2017).
16. A. Smette *et al.*, *Astron. Astrophys.* **576**, A77 (2015).
17. Materials and methods are available as supplementary materials.
18. A. Kramida, Y. Ralchenko, J. Reader, NIST ASD Team, NIST Atomic Spectra Database, version 5.5.2 (National Institute of Standards and Technology, 2018); https://physics.nist.gov/asd [accessed 2 March 2018].
19. G. Drake, *High Precision Calculations for Helium* (Springer New York, 2006), pp. 199–219.
20. D. Ehrenreich *et al.*, *Nature* **522**, 459–461 (2015).
21. A. Vidal-Madjar *et al.*, *Nature* **422**, 143–146 (2003).
22. F. Yan, T. Henning, *New Astron.* **2**, 714–718 (2018).
23. C. Moutou, A. Coustenis, J. Schneider, D. Queloz, M. Mayor, *Astron. Astrophys.* **405**, 341–348 (2003).
24. M. Salz *et al.*, *Astron. Astrophys.* 10.1051/0004-6361/201833694 (2018).
25. R. Allart *et al.*, *Science* **362**, 1384–1387 (2018).
26. N. V. Erkaev *et al.*, *Astron. Astrophys.* **472**, 329–334 (2007).
27. R. P. Butler *et al.*, *Astrophys. J.* **617**, 580–588 (2004).
28. S. Czesla, M. Salz, P. C. Schneider, M. Mittag, J. H. M. M. Schmitt, *Astron. Astrophys.* **607**, A101 (2017).
29. H. A. Knutson, A. W. Howard, H. Isaacson, *Astrophys. J.* **720**, 1569–1576 (2010).
30. B. M. Morris *et al.*, *Astrophys. J.* **848**, 58 (2017).
31. R. W. Noyes, L. W. Hartmann, S. L. Baliunas, D. K. Duncan, A. H. Vaughan, *Astrophys. J.* **279**, 763 (1984).
32. J. Sanz-Forcada, A. K. Dupree, *Astron. Astrophys.* **488**, 715–721 (2008).

ACKNOWLEDGMENTS

Parts of the results shown are based on observations obtained with XMM-Newton, an ESA science mission with instruments and contributions directly funded by ESA Member States and NASA.

We acknowledge the XMM-Newton Project Scientist for the quick and positive reaction to our request for a director's discretionary time observation of WASP-107. We thank the anonymous reviewers for their contribution to this paper. **Funding:** CARMENES is an instrument for the Centro Astronómico Hispano-Alemán de Calar Alto (CAHA, Almería, Spain). CARMENES is funded by the German Max-Planck-Gesellschaft (MPG), the Spanish Consejo Superior de Investigaciones Científicas (CSIC), the European Union through FEDER/ERF FICTS-2011-02 funds, and the members of the CARMENES Consortium (Max-Planck-Institut für Astronomie, Instituto de Astrofísica de Andalucía, Landessternwarte Königstuhl, Institut de Ciències de l'Espai, Insitut für Astrophysik Göttingen, Universidad Complutense de Madrid, Thüringer Landessternwarte Tautenburg, Instituto de Astrofísica de Canarias, Hamburger Sternwarte, Centro de Astrobiología, and Centro Astronómico Hispano-Alemán), with additional contributions by the Spanish Ministry of Economy, the German Science Foundation through the Major Research Instrumentation Programme and Deutsche Forschungsgesellschaft (DFG) Research Unit FOR2544 "Blue Planets around Red Stars," the Klaus Tschira Stiftung, the states of Baden-Württemberg and Niedersachsen, and by the Junta de Andalucía. We acknowledge funding from the Spanish Ministry of Economy and Competitiveness (MINECO) and the Fondo Europeo de Desarrollo Regional (FEDER) through grants ESP2016-80435-C2-1-R, ESP 2016-76076-R, ESP2014-54362-P, ESP 2014-54062-R, AYA2016-79425-C3-2-P, AYA2016-79425-C3-1-P, AYA2016-79425-C3-2-P, AYA2014-54348-C3-1-R, and AYA2016-79425-C3-3-P. We also acknowledge funding through the DFG through grants DFG DR281/32-1, RE 1664/14-1, DFG SFB 676, and DFG SCHM 1032/57-1 and by the Deutsches Zentrum für Luft und Raumfahrt (DLR) through grants DLR 50 OR 1710, DLR 50 OR 1307, and BMWi50OR1505, as well as the support of the Generalitat de Catalunya/CERCA program. I.A.G.S. and F.J.A.-F. acknowledge funding from the research program VICI 639.043.107 funded by the Dutch Organisation for Scientific Research (NWO) and funding from the European Research Council (ERC) under the European Union's Horizon 2020 research and innovation program under grant agreement 694513. G.C. acknowledges support by the National Natural Science Foundation of China (grant 11503088) and the Natural Science Foundation of Jiangsu Province (grant BK20151051). **Author contributions:** L.N. performed data acquisition including proposal writing and preparation of observations (DAQ), data analysis (DA), and science interpretation (SI). F.J.A.-F., F.Y., and I.A.G.S. performed DAQ, DA, and SI. E.P. and S.C. performed DAQ and SI. M.S., M.L.-P., A.S.-L., D.M., K.M., and N.C.-B. performed DA and SI. J.S.-F. performed x-ray and EUV flux modeling and calculations, DAQ, and SI. E.N. performed telluric absorption line modeling and correction. M.Z. performed DA, instrument design (ID), and official instrument pipeline design (PD). F.F.B. performed DA and PD. A.R. performed DA, ID, PD, and SI. I.R. performed ID, DAQ, and SI. A.Q. performed ID and SI. J.A.C. performed ID and DAQ. G.C. performed planet scale height calculations, DAQ, and SI. J.H.M.M.S., P.J.A., S.D., T.H., M.L., K.M., P.C.S., and M.R.Z.O. performed SI. **Competing interests:** The authors have no competing interests to declare. **Data and materials availability:** The CARMENES data are available at Centro de Astrobiología (INTA-CSIC) in the Calar Alto (CAHA) archive at http://caha.sdc.cab.inta-csic.es/calto/jsp/searchform.jsp using the following identifiers and observation dates: WASP-69: 22-23.Aug.2017 (CAHA_IDs 261990 to 262072), 22.Sep.2017 (CAHA_IDs 263371 to 263467). KELT-9b: 06-07.August.2017 (CAHA_IDs 259314 to 259424). HD209458: 16-17.Sep.2016 (CAHA_IDs 249262 to 249415) and 08.11.2016 (CAHA_IDs 251027 to 251198). The CARMENES data for GJ 436 are not yet available in the CAHA archive, so their echelle order 56, containing the He I line, is provided at http://carmenes.cab.inta-csic.es/gto/jsp/nortmannetal2018.jsp. The XMM-Newton data are archived at http://nxsa.esac.esa.int/nxsa-web/#home with the observation IDs listed in the supplementary materials. Software scripts written for the manuscript are provided in data S1.

SUPPLEMENTARY MATERIALS

www.sciencemag.org/content/362/6421/1388/suppl/DC1
Materials and Methods
Figs. S1 to S10
Tables S1 to S4
References (*33*–*74*)
Data S1

14 March 2018; accepted 16 November 2018
Published online 6 December 2018
10.1126/science.aat5348

Ground-based detection of an extended helium atmosphere in the Saturn-mass exoplanet WASP-69b

Lisa Nortmann, Enric Pallé, Michael Salz, Jorge Sanz-Forcada, Evangelos Nagel, F. Javier Alonso-Floriano, Stefan Czesla, Fei Yan, Guo Chen, Ignas A. G. Snellen, Mathias Zechmeister, Jürgen H. M. M. Schmitt, Manuel López-Puertas, Núria Casasayas-Barris, Florian F. Bauer, Pedro J. Amado, José A. Caballero, Stefan Dreizler, Thomas Henning, Manuel Lampón, David Montes, Karan Molaverdikhani, Andreas Quirrenbach, Ansgar Reiners, Ignasi Ribas, Alejandro Sánchez-López, P. Christian Schneider and María R. Zapatero Osorio

Science **362** (6421), 1388-1391.
DOI: 10.1126/science.aat5348originally published online December 6, 2018

Helium escaping from hot gas giants

Many gas giant exoplanets orbit so close to their host star that they are heated to high temperatures, causing atmospheric gases to escape. Gas giant atmospheres are mostly hydrogen and helium, which are difficult to observe. Two papers have now observed escaping helium in the near-infrared (see the Perspective by Brogi). Allart *et al.* observed helium in a Neptune-mass exoplanet and performed detailed simulations of its atmosphere, which put constraints on the escape rate. Nortmann *et al.* found that helium is escaping a Saturn-mass planet, trailing behind it in its orbit. They combined this with observations of several other exoplanets to show that atmospheres are being lost more quickly by exoplanets that are more strongly heated.

Science, this issue p. 1384, p. 1388; see also p. 1360